Cell Reports

Report

Postsynaptic neuronal activity promotes regeneration of retinal axons

Graphical abstract

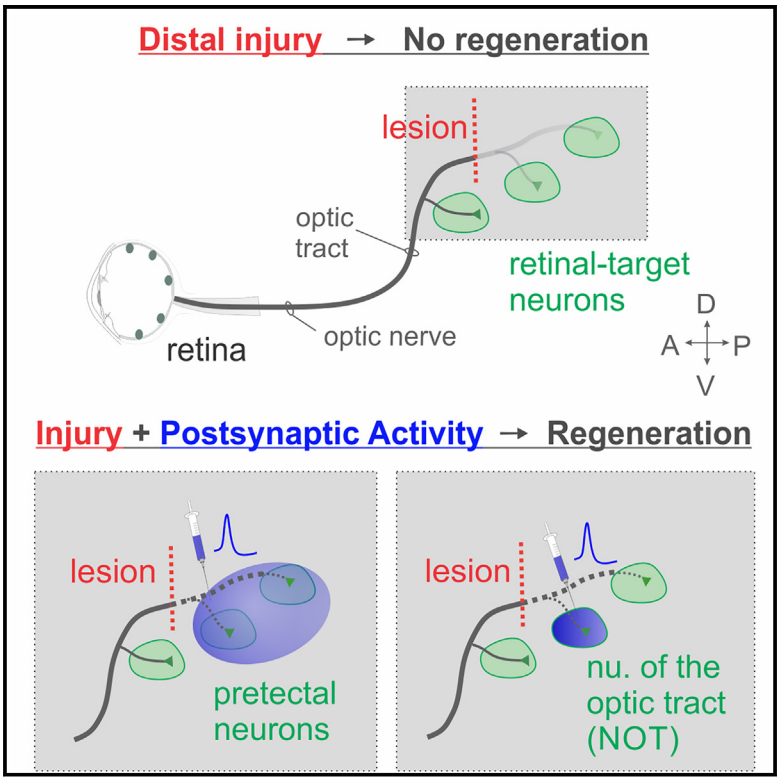

Highlights

- Neural activity in a brain target affects afferent axon regeneration
- Postsynaptic retinorecipient activity is sufficient to promote RGC regeneration
- Chronic activation of retinorecipient neuron subsets promotes axon regeneration
- Distal optic tract injury is a clinically relevant model to investigate target reinnervation

Authors

Supraja G. Varadarajan, Fei Wang, Onkar S. Dhande, Phung Le, Xin Duan, Andrew D. Huberman

Correspondence

suprajav@stanford.edu (S.G.V.), adh1@stanford.edu (A.D.H.)

In brief

Varadarajan et al. used a distal optic tract injury model to investigate the role of postsynaptic neuronal activity in promoting axon regeneration. Increasing neural activity distal to a brain lesion promotes retinal axon regeneration and target reinnervation. Selective activation of a subset of retinorecipient neurons was sufficient to promote regeneration.

Varadarajan et al., 2023, Cell Reports *42*, 112476
May 30, 2023
https://doi.org/10.1016/j.celrep.2023.112476

CellPress

Cell Reports

CellPress
OPEN ACCESS

Report

Postsynaptic neuronal activity promotes regeneration of retinal axons

Supraja G. Varadarajan,[1,*] Fei Wang,[2] Onkar S. Dhande,[1] Phung Le,[1] Xin Duan,[2,3,4] and Andrew D. Huberman[1,5,6,7,*]
[1]Department of Neurobiology, Stanford University School of Medicine, Stanford, CA, USA
[2]Department of Ophthalmology, University of California, San Francisco, San Francisco, CA, USA
[3]Department of Physiology, University of California, San Francisco, San Francisco, CA, USA
[4]Kavli Institute for Fundamental Neuroscience, University of California, San Francisco, San Francisco, CA, USA
[5]Department of Ophthalmology, Stanford University School of Medicine, Stanford, CA, USA
[6]BioX, Stanford University School of Medicine, Stanford, CA, USA
[7]Lead contact
*Correspondence: suprajav@stanford.edu (S.G.V.), adh1@stanford.edu (A.D.H.)
https://doi.org/10.1016/j.celrep.2023.112476

SUMMARY

The wiring of visual circuits requires that retinal neurons functionally connect to specific brain targets, a process that involves activity-dependent signaling between retinal axons and their postsynaptic targets. Vision loss in various ophthalmological and neurological diseases is caused by damage to the connections from the eye to the brain. How postsynaptic brain targets influence retinal ganglion cell (RGC) axon regeneration and functional reconnection with the brain targets remains poorly understood. Here, we established a paradigm in which the enhancement of neural activity in the distal optic pathway, where the postsynaptic visual target neurons reside, promotes RGC axon regeneration and target reinnervation and leads to the rescue of optomotor function. Furthermore, selective activation of retinorecipient neuron subsets is sufficient to promote RGC axon regeneration. Our findings reveal a key role for postsynaptic neuronal activity in the repair of neural circuits and highlight the potential to restore damaged sensory inputs via proper brain stimulation.

INTRODUCTION

Vision is the primary sense humans use to navigate the world and survive. Retinal ganglion cells (RGCs) are the output neurons of the eye and the sole conduit for visual information to reach the brain, where it undergoes perceptual, sensory-motor, and autonomic processing. RGCs and their axons thus represent a key bottleneck to restoring lost vision following injuries and degenerative diseases that deplete neurons, such as glaucoma. To restore vision after injury or disease, RGC axons must re-grow back into the brain and connect with specific synaptic targets, as they did in development. However, RGC axons, like all axons of the central nervous system (CNS), do not spontaneously regenerate following injury.

During development, RGC axons rely on a wide range of signals from within the retina and their central targets in the brain to wire up correctly.[1] Factors inherent to RGC axons and target-derived signals, such as axon guidance cues, trophic factors, and neural activity, direct the processes of topographic mapping, eye-specific axonal segregation, synaptic choice, synapse formation, and refinement.[2–5] Many studies have demonstrated that modifying trophic factor signaling in major central targets or ablating targets affected RGC death during development.[6–12] Target cells thus play a critical role in developing and maintaining visual circuits. Recent studies have identified strategies to increase the growth potential of RGC axons in a diseased or injured environment by recapitulating developmental mechanisms.[13,14] Most of these studies focus on molecular and cellular events in the retina and/or optic nerve. Although target neurons play an important role in the development of visual circuits, far less is known about the role of retinorecipient target cells in the regeneration process.

We used a chemogenetic approach to stimulate neural activity in specific visual target neurons following injury and evaluated how this affects RGC axon regeneration. Our findings reveal that increased neural activity in target neurons promotes RGC axon regeneration and rescues the deficits in optomotor responses typically observed following injury to the distal optic pathway. The potential to leverage postsynaptic partners of injured retinal axons to promote their regeneration and thereby restore visual system function represents an underappreciated and potentially effective strategy for repairing neural circuits.

RESULTS

Increasing neural activity in the distal optic pathway promotes RGC axon regeneration

Enhancing RGC neural activity in the retina can promote regeneration of RGC axons in an optic nerve crush model.[15,16] Here we tested the hypothesis that increasing neural activity in cells distal to the lesion site (within the brain) would promote regeneration of injured RGC axons. We used a distal-injury model in which RGC axons were unilaterally severed at a location rostral to the pretectum, resulting in a partial injury to the optic tract (Figure 1A).

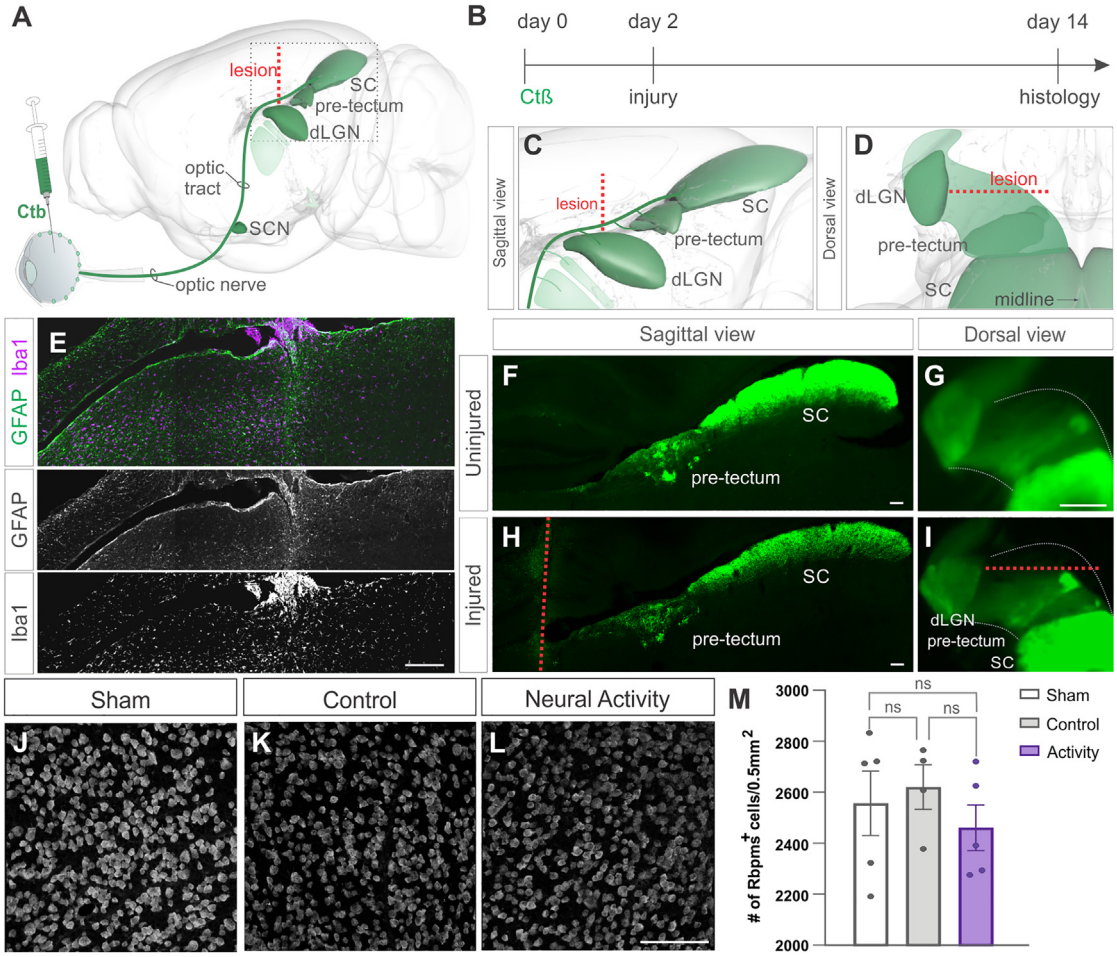

Figure 1. Injury to the distal optic tract of adult mice

(A) Schematic of distal injury (red dotted line) to the optic tract showing cholera toxin subunit b (Ctβ)-labeled RGC axon projections to central visual targets: dorsal lateral geniculate nucleus (dLGN), pretectum, superior colliculus (SC). The gray dotted rectangle shows the magnified regions shown in (C) and (D).

(B) Experimental timeline to assess the distal injury and its effect on RGC death.

(C and D) Schematic of sagittal (C) and dorsal (D) views of the optic tract and RGC projections into central visual targets.

(E) Sagittal sections demarcating the lesion area immunostained for astrocytes (GFAP, green) and microglia (IBA1, magenta).

(F–I) Sagittal (F) and dorsal (G) views of normal uninjured RGC axon projections into the pretectum and SC. Sagittal (H) and dorsal (I) views of RGC axon projections 2 weeks after distal injury. The red dotted line indicates the lesion site.

(J–M) Whole-mount retinas from sham-uninjured (J) and injured-saline-control (K), injured-CNO-activity (L) mice labeled with an RGC marker (RBPMS). Quantification of RGCs 2 weeks after distal injury from the contralateral eyes (M).

Ordinary one-way ANOVA, p = 0.5857; Tukey's multiple comparisons test, p = 0.9102, p = 0.7882, p = 0.5675. N = 5 animals/group for sham and activity; N = 4 animals for control. Error bars indicate SEM. Scale bars, 1,000 μm (G), 100 μm.

There are two advantages to using this distal-injury model for probing the role of target cells in axon regeneration: (1) a shorter distance for regenerating axons to reach their targets; (2) RGC axon collaterals innervating visual targets rostral to the lesion site would retain connectivity and trophic support and thereby minimize RGC death in the retina, a major confounding issue of optic nerve crush models.[17–19]

We first set out to determine if the distal-injury model indeed minimizes RGC death. RGC axons were visualized by labeling them with cholera toxin subunit b (Ctβ) (Figures 1A and 1B). Two days later, the distal lesion was performed to partially sever the contralateral optic tract (Figures 1C–1I). To assess RGC death induced by the lesion, we processed the retinas for immunohistochemistry using the RGC-specific marker RNA Binding Protein with Multiple Splicing (RBPMS)[20,21] (Figures 1J–1M). We observed no significant reduction in the number of RGCs compared with sham (uninjured) retinas (p = 0.5857 from one-way ANOVA with *post hoc* Tukey's multiple comparisons, n = 5 animals/group) (Figure 1M), indicating that the distal-injury model minimizes RGC death.

To test the hypothesis that stimulating postsynaptic neurons could promote RGC axon regeneration, we used a previously established chemogenetic approach to increase neural activity in pretectal neurons caudal to the lesion (Figures 2A–2F).[15,20] We

CellPress
OPEN ACCESS

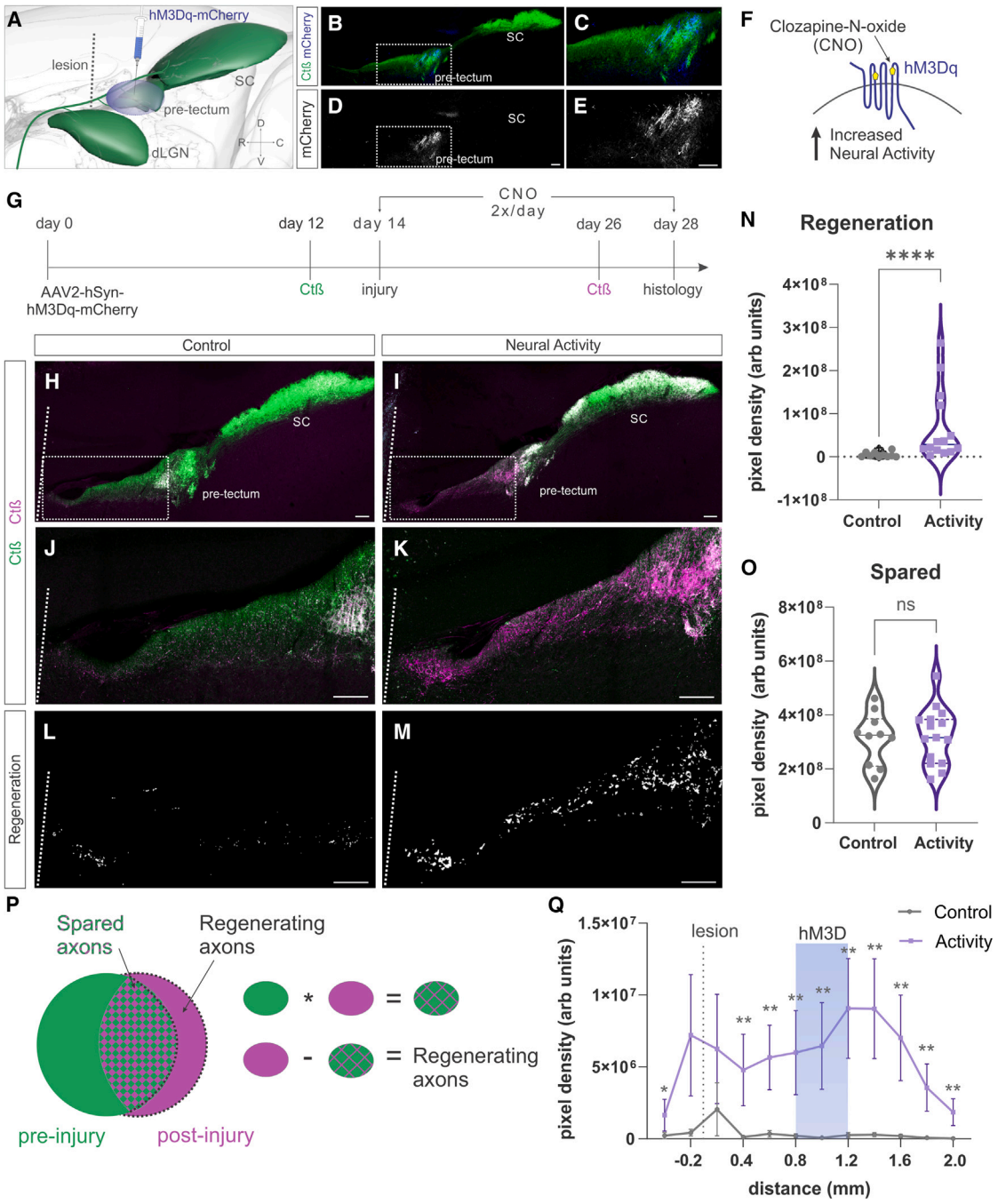

Figure 2. Non-specific stimulation of the distal optic tract promotes RGC axon regeneration

(A) Schematic of chemogenetic stimulation of neurons in the pretectum relative to the lesion site (gray dotted line).

(B–E) Ctβ-labeled RGC axon projections (green) in the pretectum and SC; mCherry-labeled neurons in the pretectum expressing hM3Dq-mCherry (blue). White dotted rectangles in (B) and (D) show magnified regions in (C) and (E), respectively.

(F) Schematic of chemogenetic stimulation: clozapine-N-oxide (CNO) binds modified hM3Dq to increase neural activity within cells.

(G) Experimental timeline for stimulating neurons in the pretectum following distal injury.

(H and I) Representative images showing Ctβ labeled RGC axon projections in the pretectum and SC. Sagittal sections of the brain with pre-injury Ctβ label (green), post-injury Ctβ label (magenta) from control (H), and neural activity groups (I). The white dotted line indicates the lesion site.

(J and K) White rectangles in (H) and (I) show magnified regions in (J) and (K), respectively.

(L and M) Images in (J) and (K) were processed to identify regenerating axons only labeled with post-injury Ctβ.

(N) Quantification of the pixel density of regenerating axons (analyzed as shown in P). Individual data points in each graph represent the sum of pixel density from one animal. Mann-Whitney test: ****$p < 0.0001$. N = 10 animals (control), 14 animals (activity).

(legend continued on next page)

overexpressed an engineered G-protein-coupled receptor hM3Dq (modified human M3 muscarinic designer receptor exclusively activated by designer drug [DREADD]) into the pretectum of 8-week-old mice using adeno-associated virus (AAV; AAV2-hSyn-hM3Dq-mCherry[22,23]) (Figure 2G). Two weeks later, the distal optic tract was lesioned, and mice were given intraperitoneal injections of either saline (control group) or the synthetic ligand clozapine-N-oxide (CNO) to activate hM3Dq (neural activity group), thereby increasing their neuronal activity[15] (Figures 2A–2F). We first confirmed hM3D activation by immunostaining for cFos, an immediate-early gene induced by neural activity.[24] Double-labeled mCherry$^+$ cFos$^+$ cells were observed 24 h following CNO injection (Figures S1D–S1F) and following a 2-week period (Figures S1J–S1L) but not after injecting saline (Figures S1A–S1C and S1G–S1I). No mCherry$^+$ cFos$^+$ cells were observed in the dorsal lateral geniculate nucleus (dLGN) or superior colliculus (SC) of CNO-injected mice (Figures S1M and S1N). Recordings from mCherry$^+$ cells showed a significant increase in the firing rate ($p = 0.019$ after adding CNO, $p = 0.0019$ after washout, from paired t test, $n = 5$ cells from three mice) and resting potential ($p = 0.0097$ from unpaired t test, $n = 5$ cells from three mice) following CNO administration (Figures S1O–S1S). A subsequent CNO washout significantly decreased the firing rate ($p = 0.0019$ from paired t test) (Figure S1Q). CNO administration was not found to exert any independent effects on regeneration and was not statistically significant compared with saline-injected controls ($p = 0.5565$ from unpaired t test, $n = 2$ animals/group) (Figure S1T). To unambiguously identify regenerating axons, mice received intravitreal injections of Ctβ conjugated to Alexa Fluor (Ctβ-647 and Ctβ-488) 2 days before the injury and 12 days after injury, respectively (Figures 2G, 2P, and S2A–S2F). Quantification of RGCs that were double labeled in the retina showed that the number of RGCs labeled with the first (91%), second (93%), or both (88%) tracers were not statistically significant, indicating adequate labeling by both tracers ($p = 0.61$ for uninjured and $p = 0.9077$ with a two-way ANOVA followed by *post hoc* Tukey's multiple comparisons, $n = 4$ animals for control and five animals for activity) (Figures S2G–S2M).

Increasing neural activity in pretectal neurons post injury for 2 weeks led to significantly greater RGC axon regeneration than was observed in control mice ($p < 0.0001$ with Mann-Whitney test, $n = 12$–15 sections/mice from 10 mice in the control group, and 14 mice in the activity group) (Figures 2H–2N). We sought to determine if a relationship exists between the proportion of RGC axons spared from injury and the degree of regeneration observed (Figure 2P). A comparison of spared axons between groups revealed no significant differences ($p = 0.8408$ with Mann-Whitney test) (Figure 2O). We found no significant difference in cell death between the control and activity groups (Figure 1M). These results suggest that the increase in regeneration is due to the enhancement of neural activity in the chemogenetically manipulated pretectal neurons.

We sought to determine the extent to which increasing activity in the pretectum could promote regeneration. HM3D-mCherry$^+$ neurons were observed throughout the pretectum but not in the dLGN or SC (Figure S3A). We measured the observed regeneration in the distal optic pathway as a function of distance. We found that, while control animals exhibited the highest degree of regeneration at only 200 μm from the lesion site, increasing neural activity promoted regeneration at all distances up to 2,000 μm from the lesion site, with the highest degree of regeneration observed at 1,400 μm from the lesion site ($p < 0.0001$ from t test with *post hoc* multiple non-parametric t tests; 12–15 sections/mice from 10 mice in the control group and 14 mice in the activity group) (Figure 2Q). Although the total pixel density of regenerating axons varied between animals, regeneration was observed in all 10 mice of the neural activity group (Figures S3B–S3S).

Regenerating axons reach target nuclei

To assess whether regenerating axons also re-innervated visual targets, we quantified the density of regenerating axons within each subcortical visual target. We focused on the pretectal targets near the hM3Dq-injection site, such as the olivary pretectal nucleus (OPN; responsible for pupillary light reflex), the nucleus of the optic tract (NOT; horizontal image stabilization), the medial division of the posterior pretectal nucleus (mdPPN; function unknown), and the SC (head and eye movements).[25] Because the lesion site was medial to the dLGN, RGC collaterals innervating the dLGN are proximal to the lesion and thus not injured; nevertheless, we expected injured axons to degenerate a few hundred micrometers from the injury site before regenerating.[14,26] Therefore, we also evaluated regeneration within the dLGN. We observed significantly more regenerating axons within all target nuclei in the neural activity group ($p < 0.001$) (Figures S4A–S4Y). We examined whether regenerating axons navigated more favorably toward one or more targets within the neural activity group. Since each visual target varies by size, we normalized the degree of regeneration within each target by the target area. We found no significant difference in regeneration between the targets (Figure S4Z) ($p = 0.185$ from ordinary one-way ANOVA with *post hoc* Tukey's multiple comparisons). These findings suggest that injured axons died back as far as the dLGN (~500 μm) and that

(O) Quantification of the pixel density of spared axons labeled with both pre-injury and post-injury Ctβ (analyzed as shown in P). Mann-Whitney test: n.s., $p = 0.8408$. $N = 10$ animals (control), 14 animals (activity).

(P) Pre-injury Ctβ label (green) and post-injury Ctβ label (magenta) injected into the eyes of mice can be processed to distinguish regenerating versus spared axons.

(Q) Quantification of regeneration as a function of distance. The average pixel density of all animals at each point on the x axis is plotted. The gray dotted line shows the lesion site, the blue bar indicates the hM3Dq-injection site.

Paired t test to compare the group as a whole: ****$p < 0.0001$. Multiple Mann-Whitney tests to compare control and activity at each individual distance: $p = 0.022$, 0.259, 0.095, 0.0038, 0.00038, 0.0059, 0.0058, 0.0047, 0.0024, 0.0059, 0.0058, and 0.0069. $N = 10$ animals (control), 14 animals (activity). Error bars indicate SEM. Scale bars, 100 μm.

See also Figures S1–S4.

regenerating axons navigated toward regions that are highly electrically active.

A genetic driver to manipulate retinorecipient cells in the NOT

To dissect the role of neural activity more specifically in postsynaptic cells that receive RGC inputs (retinorecipient cells) in regeneration, we focused on the NOT, a subcortical visual target nucleus. RGC inputs to the NOT, a component of the accessory optic system (AOS) critical for image stabilization, are required to control horizontal eye movements.[27–29] We sought mouse lines to target and manipulate the cells within the NOT selectively. We screened a library of BAC-transgenic Cre recombinase driver lines (GENSAT) and identified the Synaptotagmin 17 Cre line (*Syt17::Cre*) as a possible candidate. To characterize the Cre-labeled cells in the *Syt17::Cre* line, we crossed the mice with a reporter expressing tdTomato and examined the brains of their offspring: *Syt17::Cre; Ai9::tdTomato* (Figures S5A–S5E and S5I). We used Ctβ-488 to visualize the axons of all RGCs and retinorecipient innervation and quantitated which regions contained tdTomato$^+$ cells.

We observed tdTomato$^+$ cells within the NOT ($p = 0.0012$ from t test, n = a total of 32 sections from four animals) (Figures S5C–S5E), but none within the dLGN, mdPPN, or SC (Figures S6A–S6C and S6G–S6L). We occasionally observed a few tdTomato$^+$ cells within the OPN (Figures S5E and S6D–S6F); however, tdTomato$^+$ OPN cells were not present in all mice. We also crossed the *Syt17::Cre;Ai9* mouse line with the *Hoxd10::GFP* mouse line, which labels RGCs projecting to retinorecipient targets of the AOS, which includes the NOT, DTN, and MTN.[29] As expected from previous reports, we confirmed the presence of Ai9-tdTomato$^+$ cells in the vicinity of GFP$^+$ RGC axons within the NOT (Figures S5F–S5H). Additionally, previous reports have confirmed that RGCs are not labeled in the *Syt17::Cre* line.[30] These findings confirm that the *Syt17::Cre* mouse line is useful for labeling and manipulating NOT neurons restrictively.

Anatomically, the NOT is a target containing RGC afferents, excitatory, and inhibitory neurons that project to and receive input from other brainstem nuclei.[28,31] To confirm whether the Cre$^+$ cells in the NOT receive RGC inputs, we used pseudotyped-rabies viral tracing to label pre-synaptic inputs to Cre$^+$ cells in the NOT (Figures S5J–S5V). In this approach, the rabies virus can jump one synapse, and pre-synaptic inputs can be identified with mCherry[32,33] (Figure S5T). We analyzed sections of the brain and the retina and found mCherry$^+$ axons in the optic tract and mCherry$^+$ cells in the retina (Figures S5N–S5V). Cross sections of the retina immunostained with choline acetyltransferase (ChAT) showed that the majority of mCherry$^+$ RGCs were bistratified in the inner plexiform layer, where the dendritic arbors co-label with the ChAT layer, suggesting these RGCs may be on-off direction-selective ganglion cells or other bistratified RGC subtypes (Figures S5K–S5M).[25] Since RGCs are the only cells that extend projections out of the retina, these data confirm that Cre$^+$ cells in the *Syt17::Cre* mouse line receive monosynaptic inputs from RGCs and validate Cre$^+$ cells in the NOT as *bona fide* retinorecipient cells.

Retinorecipient target-cell activity promotes RGC axon regeneration

Non-specific activation of neurons in the pretectum included cells that receive visual information and other diverse types of neurons that do not receive visual input. Thus, we next asked if any cells distal to the lesion could be manipulated to promote regeneration or if only target activity from synaptic partners was required to promote regeneration of injured axons. We overexpressed Cre-dependent hM3Dq in the NOT of *Syt17::Cre* mice to allow for selective increase in neural activity in retinorecipient cells of the NOT (Figures 3A–3F). Cre$^-$ mice that received cre-dependent hM3Dq injections and CNO were used as controls (Figure 3B). We identified regenerating axons unambiguously using Ctβ-647 and Ctβ-488, injected before and after injury, respectively (Figures 3G and 3H). Quantitation of regenerating axon pixel density in the distal optic pathway showed that increasing neural activity selectively in Cre$^+$ cells in the NOT significantly increased RGC axon regeneration as compared with controls ($p = 0.033$ from Mann-Whitney test, n = 12–15 sections/mice from seven animals in the activity group and three animals in the control group) (Figure 3I). Measurement of the pixel density of spared axons showed no significant difference between the groups ($p > 0.99$ from Mann-Whitney test) (Figure 3J). Binning the pixel density of regenerating axons as a function of distance from the lesion site revealed that maximum regeneration caudal to the lesion was observed closest to the injection site ($p = 0.0079$ from paired t test with multiple *post hoc* t tests) (Figure 3K), indicating that regenerating axons navigate preferentially toward activity-induced signals. To determine if injured RGC axons were regrowing or if spared axons were sprouting collaterals in response to increased activity, we retrogradely labeled RGCs in the retina. We found 4-fold more GFP$^+$ RGCs in the activity group compared with controls (average 80 cells in the activity group and 20 cells in the control group, $p = 0.02$ using an unpaired t test, n = 4 animals for control and n = 3 for activity group) (Figures 3L–3N). These results suggest that retinorecipient target-cell activity is sufficient to promote RGC axon regeneration following a distal injury.

We also find that selectively stimulating retinorecipient neurons within the NOT is sufficient to promote regeneration within that target and to neighboring visual targets, albeit to a lesser degree than with non-specific pretectal activation. Quantification of regenerating axons within each target revealed significantly greater regeneration in all targets in the activity group compared with controls (Figures S7A–S7E). The average pixel density was highest within the NOT compared with other pretectal targets in the activity group (Figure S7F). However, a comparison of the pixel density of regenerating axons (normalized to the area of the corresponding targets) showed no statistically significant difference among the targets ($p = 0.0551$ from two-way ANOVA with *post hoc* Tukey's multiple comparisons) (Figure S7G). These results indicate that stimulating neurons within the NOT directed regenerating axons to the NOT and other visual targets.

Increasing neural activity rescues deficits in optomotor response induced by injury

To understand if the degree of regeneration observed was sufficient to restore function following injury, we compared the

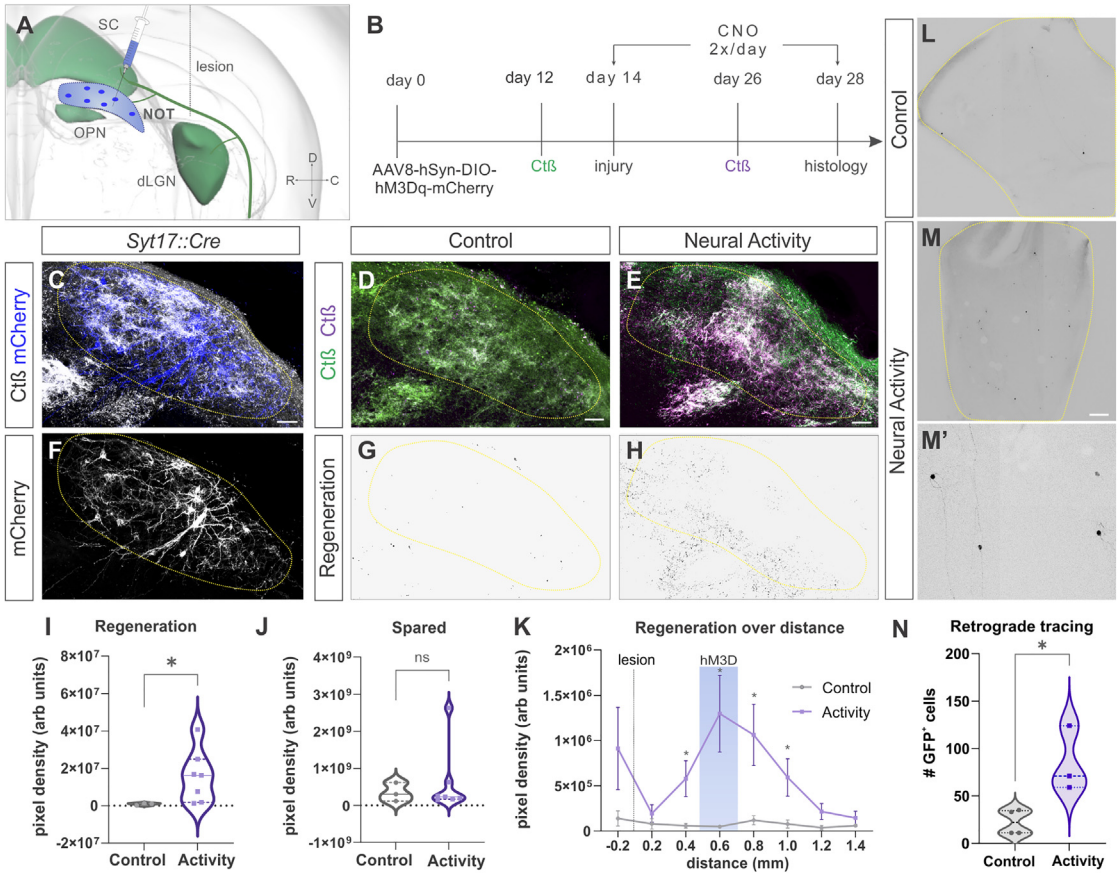

Figure 3. Selective stimulation of retinorecipient cells promotes regeneration

(A) Cre-dependent Flex-hM3Dq injected into the NOT of *Syt17::Cre* mice increases neural activity in Cre$^+$ cells postsynaptic to RGCs.

(B) Experimental timeline to stimulate NOT cells post distal injury.

(C and F) Coronal sections showing Cre+ cells in the NOT that receive Ctβ-labeled RGC input expressing hM3Dq (blue, F).

(D, E, G, and H) Representative images of coronal sections of the brain labeled with pre-injury Ctβ (green) and post-injury Ctβ (magenta) from control (D and G) and neural activity groups (E and H). Images in (D) and (E) are shown processed to identify regenerating axons (G and H, respectively).

(I) Quantification of the pixel density of regenerating axons. Individual data points represent the sum of pixel density from one animal. Mann-Whitney test: *p = 0.033. N = 3 animals (control) and N = 7 animals (activity).

(J) Quantification of the pixel density of spared axons. Individual data points represent the sum of pixel density from one animal. Mann-Whitney test: n.s. p > 0.9999. N = 3 animals (control) and N = 7 animals (activity).

(K) Quantification of the pixel density of regenerating axons as a function of distance. The average pixel density of all animals at each point on the x axis is plotted. The blue bar in K represents the hM3Dq-injection site. The gray dotted line indicates the lesion site. Paired t test to compare the group as a whole: **p = 0.0079. Multiple unpaired t tests to compare control and activity at each individual distance: p = 0.14, 0.34, 0.040, 0.025, 0.031, 0.048, 0.095, and 0.318. N = 3 animals (control) and N = 7 animals (activity). Error bars indicate SEM.

(L–N) Retinal whole mounts from control (L) and activity (M) groups show GFP$^+$ RGCs labeled via retrograde tracing from the NOT. (M′) The white box in M is magnified in M′. (N) Quantification of GFP$^+$ RGCs from both groups. Unpaired t test: *p = 0.02. N = 4 animals (control) and N = 3 animals (activity). Scale bars, 100 μm (C–E) and 200 μm (M).

See also Figures S5–S7.

optomotor reflex of animals. This assay has previously been established as a reliable way to gauge the functional recovery of RGC projections to subcortical targets in rodent models.[15,34,35] All animals generate reflexive head and eye movements in response to moving stimuli. Compensatory head movements stabilize visual images and are called optomotor responses; their generation requires multiple subcortical nuclei.[28,29,36] The visual performance or acuity of mice is determined by the spatial frequency threshold that mice can track (Figures 4A and 4B). To test for functional recovery, we increased neural activity non-specifically in the pretectum of wild-type mice. We assayed their optomotor response 2 days before and 2 weeks after the distal injury (Figure 4C). Although control mice showed a significant deficit in tracking after injury (p = 0.0081 from two-way ANOVA with *post hoc* Sidak's multiple comparisons tests, n = 5 mice), mice that had increased activity to stimulate RGC regeneration showed no significant deficit in the threshold of spatial frequency detected before and after injury (p = 0.5696, n = 6 mice; p = 0.1543 for control vs. activity post-injury response) (Figure 4D). A similar trend was observed for the length of time an animal

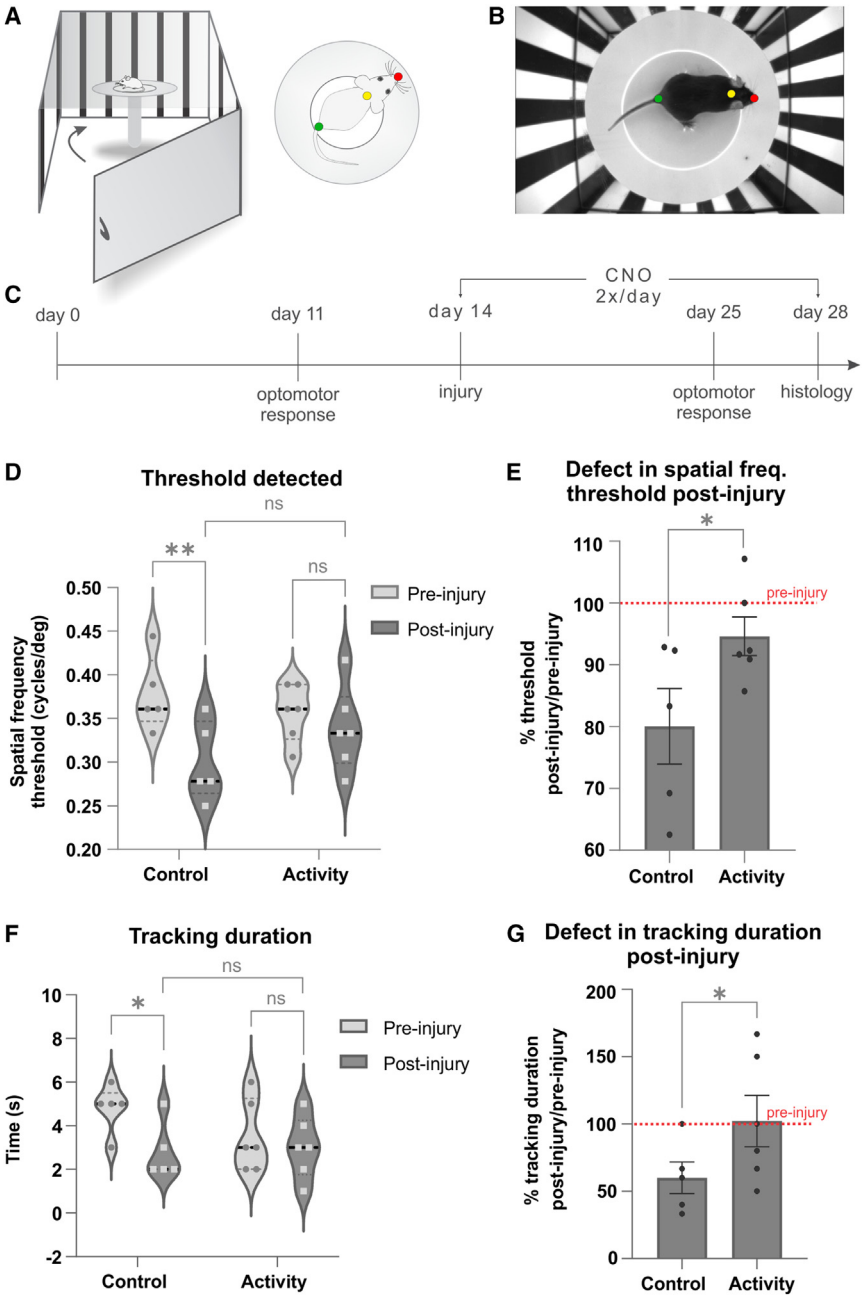

Figure 4. Increasing neural activity rescues deficit in optomotor response caused by distal injury

(A) Schematic of the OptoDrum used to measure optomotor response. The red, yellow, and green dots (right) denote head, body, and tail positions respectively.

(B) Image captured from a video shows a mouse observing low spatial frequency (0.056 cyc/deg) drifting gratings.

(C) Experimental timeline showing two recordings of optomotor response before and after injury.

(D and E) The threshold of spatial frequency tracked by each animal in control and activity groups (pre-injury, light gray; post injury, dark gray) (D). two-way ANOVA: **p = 0.0081; n.s., p = 0.5696, 0.1543. Post-injury responses normalized to pre-injury response plotted in (E). Two-way ANOVA: *p = 0.0107. N = 5 animals/group. Error bars indicate SEM. Individual data points represent one animal.

(F and G) The length of time each animal tracked the moving stimuli is shown as the tracking duration for both control and activity groups (F). Two-way ANOVA: **p = 0.0036; n.s., p = 0.5429, 0.8157. Post-injury responses normalized to pre-injury response plotted in (G). Two-way ANOVA: *p = 0.0415. N = 5 animals/group. Error bars indicate SEM. Individual data points represent one animal.

tracked the drifting gratings at the lowest spatial frequency (0.056 cycles/degree; p = 0.036 for control pre- vs. post injury, p = 0.5429 for activity pre- vs. post injury, p = 0.81 control vs. activity post-injury response from two-way ANOVA) (Figure 4F). As each animal had a slightly different threshold for tracking before injury, we normalized each animal's post-injury response as a percentage of its corresponding pre-injury response. Normalization of post-injury responses showed a significant difference between animals from the control versus activity groups in terms of threshold (p = 0.0107 from two-way ANOVA) and tracking duration (p = 0.0415 from two-way ANOVA) (Figures 4E and 4G). Taken together, these results suggest that, while a distal injury to the optic tract leads to a significant functional deficit in the optomotor response, increasing neural activity in the pretectum rescues the function of the visual circuits for reflexive image stabilization.

DISCUSSION

During development, both the retina and the postsynaptic RGC targets in the brain play crucial roles in specifying visual circuit connectivity. Previous studies have shown that ablating cellular targets in the brain or target-derived signal leads to RGC death, indicating the importance of postsynaptic RGC targets during development.[6,11] Neural activity also plays a key role in regulating transcriptional and morphological changes and trophic factor responsiveness not just during development but throughout the lifespan.[24,37–40] Here we demonstrate that activity-induced target-derived signals are essential to regenerate RGC axons in the mature brain following injury. Our findings identify two key strategies to achieve CNS circuit regeneration: (1) stimulating large collections of neurons caudal to a lesion site as a therapeutic strategy to broadly encourage regeneration of CNS axons, and (2) stimulating specific postsynaptic target neurons to promote axon regeneration in defined circuit pathways.

Attempts to repair most optic neuropathies often suffer from two major barriers: promoting regeneration of sufficient numbers of RGC axons and ensuring those extend sufficiently long distances to re-interface with their brain targets. The distal-injury model we described here—by producing a lesion to the optic tract without damaging retinorecipient target nuclei—provides a model in which the role of RGC axon-target reinnervation can be examined. RGC axons extend up to 2 mm past the injury site, a considerable distance for mature CNS axons to grow within 2 weeks, and re-connect to subcortical visual targets. In optic nerve crush models, there is profound cell death (~80%) between 1 and 3 weeks post injury.[18] It is notable that RGC death does not appear to be affected following distal-injury. This could presumably be due to the increased distance between the retina and the lesion site compared with optic nerve crush injuries. However, we cannot exclude the possibility that cell death may be stalled or occurring at a slower rate in our model.

The distal-injury model also mimics certain aspects of clinically relevant CNS diseases that manifest as axonopathy, whereby some axons are spared and others are lesioned and/or degenerate, such as in glaucoma, multiple sclerosis, amyotrophic lateral sclerosis.[41–43] Our observation that postsynaptic activity promotes RGC axon regeneration is unlikely to be the mere consequence of spared axons since there was no significant difference in the degree of sparing between groups. Further, our retrograde tracing suggest that injured RGC axons are truly regenerating (Figure 3N). We do not, however, rule out the potential role of spared axons sprouting new collaterals, or providing a structural scaffold for the regeneration of activity-stimulated axons. Pioneering axons have long been known to provide cues to guide follower axons during development.[44–49] Thus, the partial-injury model provides a tractable solution to examine multiple aspects of axon regeneration and pathfinding following injury not made possible by injury models where entire pathways are severed.

Chronic stimulation of neurons in the SC with optogenetic approaches has proven moderately neuroprotective to RGCs in a mouse glaucoma model.[50] Work in humans has identified various approaches to modulate neural activity via invasive and non-invasive approaches to treat depression, Parkinson's disease, and epilepsy.[51–56] More recently, stimulating RGCs in humans using optogenetic approaches resulted in partial functional recovery in neurodegenerative diseases such as retinitis pigmentosa.[57] With these discoveries, reapplying developmental mechanisms to restore human visual pathways and function have become fathomable.

Limitations of the study

Further studies are needed to understand the functional contribution of regenerating axons fully. Since a partial injury allows some spared axons to remain connected, tonic depolarization due to increased activity may allow spared axons to drive functional rescue. Further, retrograde tracing from the NOT to label truly regenerating RGCs only labeled a relatively small number of neurons. This is likely due to the small number of RGCs projecting to the NOT compared with major targets such as the dLGN or SC. Although this indicates that injured RGCs are regenerating in this approach, further studies are needed to identify the total number of regenerating RGCs. Although a partial injury mimics many clinically relevant injuries and is useful from a therapeutic standpoint to identify approaches that promote repair, a complete injury would provide further information regarding the potential of postsynaptic neuronal activity to promote regeneration and functional recovery in the absence of spared axons.

STAR★METHODS

Detailed methods are provided in the online version of this paper and include the following:

- KEY RESOURCES TABLE
- RESOURCE AVAILABILITY
  - Lead contact
  - Materials availability
  - Data and code availability
- EXPERIMENTAL MODEL AND SUBJECT DETAILS
  - Animals
- METHOD DETAILS
  - Intravitreal injections of tracers
  - Intraperitoneal injection of clozapine-N-oxide
  - Stereotaxic brain injections
  - Distal injury
  - Immunohistochemistry
  - c-Fos analysis
  - Electrophysiology
  - Optomotor response
  - Imaging
- QUANTIFICATION AND STATISTICAL ANALYSIS
  - Cell number quantification
  - Quantification of double-labeled RGCs
  - Quantification of regenerating and spared axons
  - Quantification of optic tract regeneration over distance
  - Statistical analysis

SUPPLEMENTAL INFORMATION

Supplemental information can be found online at https://doi.org/10.1016/j.celrep.2023.112476.

ACKNOWLEDGMENTS

We thank Drs. Alex Kolodkin, David Feldheim, and Huberman lab members for helpful discussions and comments on the manuscript. This work was supported by grants from the National Eye Institute of the NIH: RO1EY027713 and R01EY026100 (A.D.H.), RO1EY030138, and P30EY002162 (X.D.); The Gilbert Vision Restoration Initiative (A.D.H.); Catalyst for a Cure (X.D.); and Knights Templar Eye Foundation (S.G.V.).

AUTHOR CONTRIBUTIONS

S.G.V. and A.D.H. conceived and designed the experiments, and wrote the manuscript. S.G.V. performed methodology and analysis, and assembled the manuscript. S.G.V. and F.W. performed behavioral assays with X.D.'s supervision. F.W. performed electrophysiological recordings under X.D.'s supervision. O.S.D. performed histology. P.L. performed injections. The graphical abstract was designed by S.G.V.

DECLARATION OF INTERESTS

Authors declare no competing interests.

Received: June 27, 2022
Revised: November 2, 2022
Accepted: April 19, 2023
Published: May 3, 2023

REFERENCES

1. Seabrook, T.A., Burbridge, T.J., Crair, M.C., and Huberman, A.D. (2017). Architecture, function, and assembly of the mouse visual system. Annu. Rev. Neurosci. *40*, 499–538.
2. Pfeiffenberger, C., Cutforth, T., Woods, G., Yamada, J., Rentería, R.C., Copenhagen, D.R., Flanagan, J.G., and Feldheim, D.A. (2005). Ephrin-As and neural activity are required for eye-specific patterning during retinogeniculate mapping. Nat. Neurosci. *8*, 1022–1027.
3. Cang, J., and Feldheim, D.A. (2013). Developmental mechanisms of topographic map formation and alignment. Annu. Rev. Neurosci. *36*, 51–77.
4. Varadarajan, S.G., and Huberman, A.D. (2018). Assembly and repair of eye-to-brain connections. Curr. Opin. Neurobiol. *53*, 198–209.
5. Tsai, N.Y., Wang, F., Toma, K., Yin, C., Takatoh, J., Pai, E.L., Wu, K., Matcham, A.C., Yin, L., Dang, E.J., et al. (2022). Trans-Seq maps a selective mammalian retinotectal synapse instructed by Nephronectin. Nat. Neurosci. *25*, 659–674.
6. Ma, Y.T., Hsieh, T., Forbes, M.E., Johnson, J.E., and Frost, D.O. (1998). BDNF injected into the superior colliculus reduces developmental retinal ganglion cell death. J. Neurosci. *18*, 2097–2107.
7. Osborne, A., Khatib, T.Z., Songra, L., Barber, A.C., Hall, K., Kong, G.Y.X., Widdowson, P.S., and Martin, K.R. (2018). Neuroprotection of retinal ganglion cells by a novel gene therapy construct that achieves sustained enhancement of brain-derived neurotrophic factor/tropomyosin-related kinase receptor-B signaling. Cell Death Dis. *9*, 1007.
8. Pease, M.E., McKinnon, S.J., Quigley, H.A., Kerrigan-Baumrind, L.A., and Zack, D.J. (2000). Obstructed axonal transport of BDNF and its receptor TrkB in experimental glaucoma. Invest. Ophthalmol. Vis. Sci. *41*, 764–774.
9. Herzog, K.H., and von Bartheld, C.S. (1998). Contributions of the optic tectum and the retina as sources of brain-derived neurotrophic factor for retinal ganglion cells in the chick embryo. J. Neurosci. *18*, 2891–2906.
10. Quigley, H.A., McKinnon, S.J., Zack, D.J., Pease, M.E., Kerrigan-Baumrind, L.A., Kerrigan, D.F., and Mitchell, R.S. (2000). Retrograde axonal transport of BDNF in retinal ganglion cells is blocked by acute IOP elevation in rats. Invest. Ophthalmol. Vis. Sci. *41*, 3460–3466.
11. Harvey, A.R., and Robertson, D. (1992). Time-course and extent of retinal ganglion cell death following ablation of the superior colliculus in neonatal rats. J. Comp. Neurol. *325*, 83–94.
12. Bähr, M., Wizenmann, A., and Thanos, S. (1992). Effect of bilateral tectum lesions on retinal ganglion cell morphology in rats. J. Comp. Neurol. *320*, 370–380.
13. Williams, P.R., Benowitz, L.I., Goldberg, J.L., and He, Z. (2020). Axon regeneration in the mammalian optic nerve. Annu. Rev. Vis. Sci. *6*, 195–213.
14. Varadarajan, S.G., Hunyara, J.L., Hamilton, N.R., Kolodkin, A.L., and Huberman, A.D. (2022). Central nervous system regeneration. Cell *185*, 77–94.
15. Lim, J.-H.A., Stafford, B.K., Nguyen, P.L., Lien, B.V., Wang, C., Zukor, K., He, Z., and Huberman, A.D. (2016). Neural activity promotes long-distance, target-specific regeneration of adult retinal axons. Nat. Neurosci. *19*, 1073–1084.
16. Li, S., Yang, C., Zhang, L., Gao, X., Wang, X., Liu, W., Wang, Y., Jiang, S., Wong, Y.H., Zhang, Y., and Liu, K. (2016). Promoting axon regeneration in the adult CNS by modulation of the melanopsin/GPCR signaling. Proc. Natl. Acad. Sci. USA *113*, 1937–1942.
17. Tran, N.M., Shekhar, K., Whitney, I.E., Jacobi, A., Benhar, I., Hong, G., Yan, W., Adiconis, X., Arnold, M.E., Lee, J.M., et al. (2019). Single-cell profiles of retinal ganglion cells differing in resilience to injury reveal neuroprotective genes. Neuron *104*, 1039–1055.e12.
18. Duan, X., Qiao, M., Bei, F., Kim, I.-J., He, Z., and Sanes, J.R. (2015). Subtype-specific regeneration of retinal ganglion cells following axotomy: effects of osteopontin and mTOR signaling. Neuron *85*, 1244–1256.
19. Park, K.K., Liu, K., Hu, Y., Smith, P.D., Wang, C., Cai, B., Xu, B., Connolly, L., Kramvis, I., Sahin, M., and He, Z. (2008). Promoting axon regeneration in the adult CNS by modulation of the PTEN/mTOR pathway. Science *322*, 963–966.
20. Seabrook, T.A., Dhande, O.S., Ishiko, N., Wooley, V.P., Nguyen, P.L., and Huberman, A.D. (2017). Strict independence of parallel and poly-synaptic axon-target matching during visual reflex circuit assembly. Cell Rep. *21*, 3049–3064.
21. Rodriguez, A.R., de Sevilla Müller, L.P., and Brecha, N.C. (2014). The RNA binding protein RBPMS is a selective marker of ganglion cells in the mammalian retina. J. Comp. Neurol. *522*, 1411–1443.
22. Urban, D.J., and Roth, B.L. (2015). DREADDs (designer receptors exclusively activated by designer drugs): chemogenetic tools with therapeutic utility. Annu. Rev. Pharmacol. Toxicol. *55*, 399–417.
23. Krashes, M.J., Koda, S., Ye, C., Rogan, S.C., Adams, A.C., Cusher, D.S., Maratos-Flier, E., Roth, B.L., and Lowell, B.B. (2011). Rapid, reversible activation of AgRP neurons drives feeding behavior in mice. J. Clin. Invest. *121*, 1424–1428.
24. Yap, E.-L., and Greenberg, M.E. (2018). Activity-regulated transcription: bridging the gap between neural activity and behavior. Neuron *100*, 330–348.
25. Dhande, O.S., Stafford, B.K., Lim, J.-H.A., and Huberman, A.D. (2015). Contributions of retinal ganglion cells to subcortical visual processing and behaviors. Annu. Rev. Vis. Sci. *1*, 291–328.
26. Kerschensteiner, M., Schwab, M.E., Lichtman, J.W., and Misgeld, T. (2005). In vivo imaging of axonal degeneration and regeneration in the injured spinal cord. Nat. Med. *11*, 572–577.
27. Hamilton, N.R., Scasny, A.J., and Kolodkin, A.L. (2021). Development of the vertebrate retinal direction-selective circuit. Dev. Biol. *477*, 273–283.
28. Simpson, J.I. (1984). The accessory optic system. Annu. Rev. Neurosci. *7*, 13–41.
29. Dhande, O.S., Estevez, M.E., Quattrochi, L.E., El-Danaf, R.N., Nguyen, P.L., Berson, D.M., and Huberman, A.D. (2013). Genetic dissection of retinal inputs to brainstem nuclei controlling image stabilization. J. Neurosci. *33*, 17797–17813.
30. Martersteck, E.M., Hirokawa, K.E., Evarts, M., Bernard, A., Duan, X., Li, Y., Ng, L., Oh, S.W., Ouellette, B., Royall, J.J., et al. (2017). Diverse central projection patterns of retinal ganglion cells. Cell Rep. *18*, 2058–2072.
31. Lilley, B.N., Sabbah, S., Hunyara, J.L., Gribble, K.D., Al-Khindi, T., Xiong, J., Wu, Z., Berson, D.M., and Kolodkin, A.L. (2019). Genetic access to neurons in the accessory optic system reveals a role for Sema6A in midbrain circuitry mediating motion perception. J. Comp. Neurol. *527*, 282–296.
32. Kim, E.J., Jacobs, M.W., Ito-Cole, T., and Callaway, E.M. (2016). Improved monosynaptic neural circuit tracing using engineered rabies virus glycoproteins. Cell Rep. *15*, 692–699.
33. Wall, N.R., Wickersham, I.R., Cetin, A., De La Parra, M., and Callaway, E.M. (2010). Monosynaptic circuit tracing in vivo through Cre-dependent targeting and complementation of modified rabies virus. Proc. Natl. Acad. Sci. USA *107*, 21848–21853.
34. de Lima, S., Koriyama, Y., Kurimoto, T., Oliveira, J.T., Yin, Y., Li, Y., Gilbert, H.-Y., Fagiolini, M., Martinez, A.M.B., and Benowitz, L. (2012). Full-length axon regeneration in the adult mouse optic nerve and partial recovery of simple visual behaviors. Proc. Natl. Acad. Sci. USA *109*, 9149–9154.
35. Bei, F., Lee, H.H.C., Liu, X., Gunner, G., Jin, H., Ma, L., Wang, C., Hou, L., Hensch, T.K., Frank, E., et al. (2016). Restoration of visual function by enhancing conduction in regenerated axons. Cell *164*, 219–232.

36. Huberman, A.D., and Niell, C.M. (2011). What can mice tell us about how vision works? Trends Neurosci. *34*, 464–473.

37. Ackman, J.B., Burbridge, T.J., and Crair, M.C. (2012). Retinal waves coordinate patterned activity throughout the developing visual system. Nature *490*, 219–225.

38. Majdan, M., and Shatz, C.J. (2006). Effects of visual experience on activity-dependent gene regulation in cortex. Nat. Neurosci. *9*, 650–659.

39. Catalano, S.M., and Shatz, C.J. (1998). Activity-dependent cortical target selection by thalamic axons. Science *281*, 559–562.

40. Weliky, M., and Katz, L.C. (1999). Correlational structure of spontaneous neuronal activity in the developing lateral geniculate nucleus in vivo. Science *285*, 599–604.

41. Coleman, M.P., and Perry, V.H. (2002). Axon pathology in neurological disease: a neglected therapeutic target. Trends Neurosci. *25*, 532–537.

42. Krauss, R., Bosanac, T., Devraj, R., Engber, T., and Hughes, R.O. (2020). Axons matter: the promise of treating neurodegenerative disorders by targeting SARM1-mediated axonal degeneration. Trends Pharmacol. Sci. *41*, 281–293.

43. Fischer, L.R., Culver, D.G., Tennant, P., Davis, A.A., Wang, M., Castellano-Sanchez, A., Khan, J., Polak, M.A., and Glass, J.D. (2004). Amyotrophic lateral sclerosis is a distal axonopathy: evidence in mice and man. Exp. Neurol. *185*, 232–240.

44. Raper, J., and Mason, C. (2010). Cellular strategies of axonal pathfinding. Cold Spring Harb. Perspect. Biol. *2*, a001933.

45. Osterhout, J.A., El-Danaf, R.N., Nguyen, P.L., and Huberman, A.D. (2014). Birthdate and outgrowth timing predict cellular mechanisms of axon target matching in the developing visual pathway. Cell Rep. *8*, 1006–1017.

46. McConnell, S.K., Ghosh, A., and Shatz, C.J. (1989). Subplate neurons pioneer the first axon pathway from the cerebral cortex. Science *245*, 978–982.

47. Klose, M., and Bentley, D. (1989). Transient pioneer neurons are essential for formation of an embryonic peripheral nerve. Science *245*, 982–984.

48. Sitko, A.A., Kuwajima, T., and Mason, C.A. (2018). Eye-specific segregation and differential fasciculation of developing retinal ganglion cell axons in the mouse visual pathway. J. Comp. Neurol. *526*, 1077–1096.

49. Pittman, A.J., Law, M.-Y., and Chien, C.-B. (2008). Pathfinding in a large vertebrate axon tract: isotypic interactions guide retinotectal axons at multiple choice points. Development *135*, 2865–2871.

50. Geeraerts, E., Claes, M., Dekeyster, E., Salinas-Navarro, M., De Groef, L., Van den Haute, C., Scheyltjens, I., Baekelandt, V., Arckens, L., and Moons, L. (2019). Optogenetic stimulation of the superior colliculus confers retinal neuroprotection in a mouse glaucoma model. J. Neurosci. *39*, 2313–2325.

51. Cagnan, H., Denison, T., McIntyre, C., and Brown, P. (2019). Emerging technologies for improved deep brain stimulation. Nat. Biotechnol. *37*, 1024–1033.

52. Skarpaas, T.L., Jarosiewicz, B., and Morrell, M.J. (2019). Brain-responsive neurostimulation for epilepsy (RNS® System). Epilepsy Res. *153*, 68–70.

53. Krauss, J.K., Lipsman, N., Aziz, T., Boutet, A., Brown, P., Chang, J.W., Davidson, B., Grill, W.M., Hariz, M.I., Horn, A., et al. (2021). Technology of deep brain stimulation: current status and future directions. Nat. Rev. Neurol. *17*, 75–87.

54. Gall, C., Schmidt, S., Schittkowski, M.P., Antal, A., Ambrus, G.G., Paulus, W., Dannhauer, M., Michalik, R., Mante, A., Bola, M., et al. (2016). Alternating current stimulation for vision restoration after optic nerve damage: a randomized clinical trial. PLoS One *11*, e0156134.

55. Sabel, B.A., Thut, G., Haueisen, J., Henrich-Noack, P., Herrmann, C.S., Hunold, A., Kammer, T., Matteo, B., Sergeeva, E.G., Waleszczyk, W., and Antal, A. (2020). Vision modulation, plasticity and restoration using non-invasive brain stimulation - an IFCN-sponsored review. Clin. Neurophysiol. *131*, 887–911.

56. Roska, B., and Sahel, J.-A. (2018). Restoring vision. Nature *557*, 359–367.

57. Sahel, J.-A., Boulanger-Scemama, E., Pagot, C., Arleo, A., Galluppi, F., Martel, J.N., Esposti, S.D., Delaux, A., de Saint Aubert, J.-B., de Montleau, C., et al. (2021). Partial recovery of visual function in a blind patient after optogenetic therapy. Nat. Med. *27*, 1223–1229.

58. Callaway, E.M., and Luo, L. (2015). Monosynaptic circuit tracing with glycoprotein-deleted rabies viruses. J. Neurosci. *35*, 8979–8985.

59. Benkner, B., Mutter, M., Ecke, G., and Münch, T.A. (2013). Characterizing visual performance in mice: an objective and automated system based on the optokinetic reflex. Behav. Neurosci. *127*, 788–796.

60. Qi, Y., Yu, T., Xu, J., Wan, P., Ma, Y., Zhu, J., Li, Y., Gong, H., Luo, Q., and Zhu, D. (2019). FDISCO: advanced solvent-based clearing method for imaging whole organs. Sci. Adv. *5*, eaau8355.

61. Cross, T., Navarange, R., Son, J.-H., Burr, W., Singh, A., Zhang, K., Rusu, M., Gkoutzis, K., Osborne, A., and Nieuwenhuis, B. (2021). Simple RGC: ImageJ plugins for counting retinal ganglion cells and determining the transduction efficiency of viral vectors in retinal wholemounts. J. Open Res. Softw. *9*, 15.

STAR★METHODS

KEY RESOURCES TABLE

REAGENT or RESOURCE	SOURCE	IDENTIFIER
Antibodies		
Guinea pig Rbpms	Phosphosolutions	Cat#: 1832_RBPMS; RRID: AB_2492226
Rabbit DsRed	Clontech	Cat# 632496
Goat GFP	Abcam	Cat# ab6661; RRID: AB_305643
Goat ChAT	Millipore	Cat# AB144P; RRID: AB_2079751
Chicken GFAP	Aves	Cat# GFAP; RRID: AB_2313547
Goat IBA1	Abcam	Cat# ab5076; RRID: AB_2224402
Rabbit cFos	Millipore	Cat# ABE457; RRID: AB_2631318
Rabbit GFP	Thermo Fisher Scientific	Cat# A-6455; RRID: AB_221570
Bacterial and virus strains		
AAV2-hSyn-hM3Dq-mCherry	Krashes MJ et al.[23]	Addgene; Cat#50474
AAV2-hSyn-DIO-hM3Dq-mCherry	Krashes MJ et al.[23]	Addgene; Cat# 44361
AAV8-hSyn-flex-TVA-P2A-EGFP-2A-oG	Salk Vector Core	Cat# 85225
ENVA-DG-Rabies-mCherry	Salk Vector Core	Cat# 32636
G-del-Rabies-GFP	Salk Vector Core	Cat# 32635
Chemicals, peptides, and recombinant proteins		
Alexa Fluor 647-conjugated Cholera Toxin Subunit B	Thermo Fisher	Cat# C34778
Alexa Fluor 488-conjugated Cholera Toxin Subunit B	Thermo Fisher	Cat# C34775
Clozapine N-oxide (CNO)	Tocris	Cat# 4936
Experimental models: Organisms/strains		
Mouse: C57BL/6J	Jackson Laboratory	RRID: IMSR_JAX:000664
Mouse: Ai9	Jackson Laboratory	RRID: IMSR_JAX:007909
Mouse: Syt17::cre	Gensat	RRID: MMRRC_034355-UCD
Software and algorithms		
ImageJ	NIH	https://imagej.nih.gov/ij
CorelDraw X6	CorelDraw	https://www.coreldraw.com/en/
Prism 9	GraphPad Software	https://www.graphpad.com/

RESOURCE AVAILABILITY

Lead contact

Further information and requests for resources and reagents should be directed to and will be fulfilled by the lead contact, Andrew Huberman (adh1@stanford.edu).

Materials availability

This study did not generate any unique reagents.

Data and code availability

Data reported in this paper will be shared by the lead contact upon request.

This paper does not report original code.

Any additional information required to reanalyze the data reported in this paper is available from the lead contact upon request.

EXPERIMENTAL MODEL AND SUBJECT DETAILS

Animals

Mice of either sex were used and ranged from 7 to 8 weeks old. C57Bl/6J wildtype mice and Ai9-tdTomato lines were obtained from Jackson Laboratories (stock no. #000664, stock no.#007909), and *Syt17::Cre* line from (GENSAT # RRID:MMRRC_034355-UCD.

Animals were housed on a 12-h light/dark cycle with unrestricted access to food and water. All animal care and experimental procedures were conducted in accordance with NIH guidelines and as approved by the Institutional Animal Care and Use Committee at Stanford University School of Medicine and University of California, San Francisco.

METHOD DETAILS

Intravitreal injections of tracers

The following anterograde tracers were injected into the vitreal chamber of the left eye of anesthetized mice using a glass micropipette (Drummond #5-000-1001-X10):1–2 μL cholera toxin subunit-β (Ctβ) conjugated to Alexa Fluor 488 (Ctβ-488; Invitrogen #C22841) and Alexa Fluor 647 (Ctβ-647; Invitrogen #C34778) to label RGC axons. Ctβ-injected mice were given 2 days to allow the tracer to travel into the brain to label RGC axons.

Intraperitoneal injection of clozapine-N-oxide

Clozapine-N-oxide (CNO) (Tocris Bioscience #4936) was dissolved at 1 mg/ml in DMSO (0.5% saline) and administered at 1.5 mg/kg via intraperitoneal injections twice a day, 8hrs apart, for two weeks.

Stereotaxic brain injections

Mice were anesthetized with 1.5–3% isoflurane. A midline scalp incision was made to expose the skull and perform a craniotomy above the injection site. Stereotaxic injections of the virus (~0.4 μL) AAV2-hSyn-hM3Dq-mCherry (Addgene #50474[23]) were injected into the pretectum (bregma: −2.7 mm, midline: 0.8 mm, dorsal surface: 2.25mm) of 7–8 week old wildtype mice using a Nanoject II (Drummond) injector. Control mice were also injected with the same AAV-hM3Dq virus but administered saline instead of CNO. One cohort of mice was used to evaluate the independent effects of CNO, where one group of mice received AAV-hM3Dq injections followed by i.p. injections of saline (control). In contrast, another group of mice received AAV-GFP injections followed by i.p. injections of CNO (CNO) twice a day for two weeks. *Syt17::Cre* mice were injected with a Cre-dependent virus (~0.4 μL) of AAV2-hSyn-DIO-hM3Dq-mCherry (Addgene #44361[23]) into the NOT (bregma: −2.8 mm, midline: 1.0mm, dorsal surface: 2.25mm). Cre-negative mice injected with the same Cre-dependent AAV-hM3Dq virus and receiving CNO injections were used as controls for the cre experiments in Figures 3 and S7. To prevent backflow, the needles were left in place for 10 min following injections before slowly retracting to the surface.

To determine inputs to Cre-labeled cells in the NOT of *Syt17::Cre* mice, stereotaxic injections of the helper virus AAV8-hSyn-FLEX-TVA-P2A-GFP-2A-oG (0.4 μL Salk Institute #85225) was injected into the NOT of 9-week old mice. Injected mice were given three weeks for adequate expression of Cre-dependent TVA and G protein in starter cells and then injected with EnVA-ΔG-rabies-mCherry (0.35 μL Salk Institute #32636). EnVA can only bind TVA-expressing starter cells, ensuring expression only in Cre-labeled cells; the rabies virus acquires the G-glycoprotein expressed in starter cells to spread trans-synaptically, thus also preventing the spread of rabies virus beyond one synapse.[58] For retrograde tracing to identify regenerating versus spared axons, ΔG-rabies-GFP (0.35 μL Salk Institute #32635) was injected into the NOT nine days after injury. Rabies-injected mice were housed in the bio-safety cabinet for 6 days to allow adequate transsynaptic spread before analysis.

Distal injury

9-10 week old mice were anesthetized with 1.5–3% isoflurane. The midline incision made during virus injections was reopened, and scar tissue was cleared. Craniotomy was performed by drilling 3–4 burr holes using a 500 μm drill-bit (Fine Science Tools, #19007-05) and joining the individual drill sites to make a contiguous hole (bregma: −2.0 mm, midline: 0.5–2.5 mm, dorsal surface: 2.7 mm). A horizontal line was drawn using a surgical pen on a sterile surgical blade (11, Feather #2976#11) to mark the maximum depth of insertion, and then attached to a scalpel and inserted severing the optic tract from lateral to medial. Bleeding was controlled using sterile surgical spears (Sugi #30601), and the craniotomy was covered with Bone wax (Ethicon #W31G). Mice were administered with slow-release buprenorphine and/or carprofen post-surgery as needed.

Immunohistochemistry

Mice were transcardially perfused with PBS followed by 4% paraformaldehyde (PFA), and brains were harvested and postfixed in 4% PFA (24 h at 4°C). Postfixed brains were sectioned using a microtome in the sagittal or coronal plane to yield 45μm thick sections following cryoprotection with 30% sucrose in PBS. Eyes were removed, postfixed in 4% PFA (2 h at 4°C), and dissected to remove the retina was dissected, and relieving cuts were made to allow the retina to lay flat. Samples were incubated in blocking buffer (5% normal donkey serum, 0.5% Triton X-100 in PBS) for 1–2 h at room temperature. Sections were incubated overnight at 4°C in primary antibodies, while whole-mount retinas were incubated for 2 days at 4°C. The samples were washed with PBS 3x and incubated for 2 h at room temperature with secondary antibodies. Samples were mounted with Prolong Gold Antifade Medium or Vectashield. Primary antibodies were guinea pig anti-RBPMS (Phosphosolutions #1832; 1:500), rabbit anti-DsRed to enhance tdTomato (Clontech #632496, 1:2000), goat anti-GFP (Abcam #ab6673, 1:2000), goat anti-ChAT (Millipore #AB144P, 1:100), chicken anti-GFAP (Aves #ab_2313547, 1:1000), goat anti-IBA1 (Abcam #ab5076, 1:500), rabbit anti-cFos (Millipore #abe457, 1:1000), rabbit anti-GFP (Invitrogen #A-6455, 1:1000). Species-specific secondary antibodies conjugated to Alexa Fluor 594 or 647 (1:1000, Invitrogen and Jackson Laboratories) were used.

c-Fos analysis

AAV-hSyn-DIO-hM3Dq-mCherry was injected into the NOT of *Syt17::Cre*$^{+}$ mice. Two weeks later, one cohort of mice (24-h time point) received i.p. injections of CNO (1.5 mg/ml, activity group) or saline (control) twice a day, while a second cohort of mice (2-week time point) received i.p. injections of CNO or saline twice a day for two weeks. At the end of the respective timepoints, mice were housed in the dark overnight, injected with CNO, kept in the dark, and transcardially perfused 60 min after receiving CNO.

Electrophysiology

For confirming hM3Dq activation by CNO, pretectal neurons labeled with mCherry were targeted for whole-cell recording.[5] Briefly, mice were anesthetized with ketamine and xylazine (100 mg kg−1, 12.5 mg kg−1) and transcardially perfused with ice-cold cutting solution (78.3 mM NaCl, 2.3 mM KCl, 33.8 mM Choline-Cl, 0.45 mM CaCl2, 6.4 mM MgCl2, 1.1 mM NaH2PO4, 23 mM NaHCO3, 20 mM D-glucose, 0.5 mM L-glutamine, pH 7.4). The brains were dissected, and coronal sections of 250 μm thickness were prepared using a vibratome (VT1200S, Leica). Sections containing labeling in the pretectum were transferred to a chamber filled with cutting solution and incubated for 30 min at 32.5°C. After incubation, slices were transferred to artificial cerebrospinal fluid (ACSF) (125 mM NaCl, 2.5 mM KCl, 1.25 mM NaH2PO4, 26 mM NaHCO3, 1 mM MgCl2.6H2O, 2 mM CaCl2, 20 mM D-glucose, pH 7.4) and continuously bubbled with 5% CO_2/95%O_2. The current clamp mode was used to record the action potentials and resting membrane potentials of mCherry^{+} neurons in the pretectum. Spontaneous firing and resting membrane potential were recorded for 2 min before adding CNO. After bath perfusion with CNO (10μM) in ACSF for 3 min, the CNO was washed out, and the recording continued for another several minutes to observe the washout effects.

Optomotor response

The OptoDrum (Striatech Inc, Germany) was used to assay the visual behavioral response. The OptoDrum comprises a closed box with four digital displays to simulate drifting gratings. A camera attached to the top of the box records the animals' movements. At the same time, the fully-automated software was used to present the gratings, determine the spatial-frequency threshold and score the tracking performance.[59] Mice were first acclimated to the room in their cages for 30 min. Following the acclimation period, freely behaving mice were placed on a platform and allowed to acclimate to the chamber for 5 min. The fully-automated software overlays the red, yellow, and green dots (right) to denote head, body, and tail positions. Briefly, drifting gratings (12 °/s) in the clockwise direction, to gauge left-eye movements contralateral to the injury site, were presented from low spatial frequencies (0.056 cyc/deg), and the mouse was allowed to track the stimulus. To determine the threshold an animal could track, the software alternated between stimuli with high spatial frequencies (0.3–0.5 cyc/deg) and low spatial frequencies (0.06–0.1 cyc/deg) until the animal could no longer track beyond a particular frequency. Two "tracked" scores for a particular frequency and three "not-tracked" scores for the next higher frequency were determined as the threshold the animal could track. Stimuli were only presented for 3–5 s at a time and only if the animals' position was in the center of the stage/circle to avoid adaptation. Each animal was tested for 5–10 min. The stimulus was paused if an animal engaged in grooming behavior and resumed when the animal stopped grooming. False positives were identified manually and marked as invalid immediately, allowing the software to retest the same frequency or the next appropriate frequency. For defect percentage normalizing post-injury response to pre-injury responses, pre-injury responses were scored as 100, and post-injury responses were calculated as a percentage of the pre-injury response for each animal in each group. The assay was performed double-blind.

Imaging

All images were obtained with a Zeiss LSM 880 Airyscan confocal microscope or a Zeiss AxioScan microscope. Tissue collected separately for imaging purposes was cleared using the F-DISCO protocol,[60] and imaged using the LaVision Light Sheet Microscope from the Stanford Neuroscience Microscopy Service.

QUANTIFICATION AND STATISTICAL ANALYSIS

Cell number quantification

For RBPMS counts, four images were acquired from each quadrant of flat-mount retinas, and cells were counted manually for Figure S2. An automated plugin for FIJI (Simple RGC counter and Batch[61] was used to count RBPMS^{+} cells for images analyzed in Figure 1. For tdTomato^{+} cells, all sections containing the NOT and OPN were imaged for each animal (n = 5 mice), and tdTomato^{+} cells lying within the NOT/OPN were manually counted. The NOT/OPN was identified using landmark structures and confirmed by densely populated Ctβ-labeled RGC axons.[20]

Quantification of double-labeled RGCs

To measure the number of RGCs labeled with both Ctβ tracers whole-mount retinas from uninjured and injured mice injected with Ctβ-488 and Ctβ-647 two weeks apart were collected and immunostained for RBPMS. The RBPMS+ cells were counted as having one, or both tracers.

Quantification of regenerating and spared axons

Ctβ conjugated to Alexa Fluor 647 was injected intravitreally into the left eye two days prior to the distal injury to label the intact visual pathway, i.e., all RGC axons. Ctβ conjugated to Alexa Fluor 488 was injected intravitreally into the same eye twelve days after distal injury to label RGC axons that are connected to the retina: axons spared from injury would take up both Ctβ tracers and be visible at both wavelengths, whereas injured axons that are regenerating would only be labeled with the post-injury Ctβ-488 label. All images have been pseudocolored with appropriate colors for clarity.

To quantify regenerating and spared axons, confocal images of brain sections were processed through an ImageJ Macro written for this purpose (Distal cut macro), available upon request. The macro was used to split the channels in the image, perform thresholding, despeckling, and then multiply the resulting red and green channels to generate a 'yellow' image that only displays pixels in both the red and green channels, indicating these are spared axons. The 'yellow' image was then subtracted from the red channel to generate a 'red-only' image that displays uniquely-red pixels, i.e., ''regenerating axons.'' The raw integrated pixel density was measured in ImageJ from each newly generated image for each section, summed together for each animal, and then averaged. To measure regeneration within targets, a polygon outline was first drawn around each target on the merged image as regions of interest (ROI), processed through the same macro, and the raw integrated density for each ROI was measured.

Quantification of optic tract regeneration over distance

To quantify regeneration as a function of distance from the lesion ('0 mm'), the same images were binned by 200 μm blocks, measuring up to 400 μm proximal to the lesion and up to 2000 μm distal the lesion site. Images from the non-specific activation experiments are in the sagittal plane. In contrast, images from the Cre-specific activation are in the coronal plane and were accordingly measured to reflect distance from the lesion. The images were processed through an ImageJ plugin written for this purpose (Distal Cut Processor), and raw integrated density was measured within each bin. All analyses were performed blind.

Statistical analysis

To determine statistical significance, we used the Mann-Whitney t test to compare two groups of mice. Due to the variation in sample sizes, a non-parametric test was used. two-way ANOVA and One-Way ANOVA were used for distance and normalized area quantification, respectively, followed by Student's t-test on individual pairs. Two-way repeated-measures ANOVA was used with posthoc multiple comparisons for the optomotor response analysis. All statistical analysis was performed with Prism v9 (GraphPad). All data in the graphs represent mean ± SEM. Significance levels are indicated: *$p < 0.05$, **$p < 0.005$, ***$p < 0.0005$.